# Reduced dimensionality and magnetic frustration in $KCr_3As_3$

Chao Cao,[1,*] Hao Jiang,[2] Xiao-Yong Feng,[1] and Jianhui Dai[1,†]

[1]*Condensed Matter Group, Department of Physics, Hangzhou Normal University, Hangzhou 310036, People's Republic of China*

[2]*Department of Physics, Zhejiang University, Hangzhou 310013, People's Republic of China*

(Received 25 May 2015; revised manuscript received 13 October 2015; published 4 December 2015)

We study the electronic and magnetic structures of the newly discovered compound $KCr_3As_3$. The nonmagnetic state has five Fermi surface sheets involving three quasi-one-dimensional and two three-dimensional energy bands. However, the ground state is magnetic, exhibiting an interlayer antiferromagnetic order where the basic block-spin state of a unit Cr triangle retains a high spin magnitude. Moreover, the magnetic Fermi surface involves three one-dimensional sheets only, manifesting the reduced dimensionality. By fitting a twisted spin tube model, the magnetic frustrations are found to be relaxed, leading to gapless spin excitations. A frustration-induced transition to the disordered low block-spin state is expected upon increasing the intralayer exchange interaction.

DOI: 10.1103/PhysRevB.92.235107 PACS number(s): 75.10.Pq, 75.50.Lk, 75.70.Tj

## I. INTRODUCTION

The interplay between the superconductivity and magnetism or other competing density waves has been a major theme in modern condensed matter physics, particularly in the transition metal compounds with both strong electron correlations and reduced dimensionality. Although the development of long-range orders at finite temperature is forbidden in strictly one-dimensional systems with short-range interactions [1,2], such restriction can be lifted for quasi-one-dimensional (Q1D) systems. Typical examples include the Q1D superconductors $(TMTSF)_2X$ [3], $M_2Mo_6Se_6$ ($M$ = Tl,In) [4], $Li_{0.9}Mo_6O_{17}$ [5,6], etc. A universal phase diagram for the Q1D superconductors suggests that the superconductivity is in close proximity to the density waves [7,8].

The recently discovered Q1D superconductors $A_2Cr_3As_3$ ($A$ = K, Rb, Cs) has provided a new setting for understanding the interplay of the unconventional superconductivity and the density-wave instabilities at reduced dimensions [9–11]. The building blocks of these compounds consist of Q1D $[CrAs]_\infty$ double-wall nanotubes intercalated by $A^+$ cations. The first-principles calculations using the density-functional theory (DFT) [12,13] predicted a three-dimensional (3D) Fermi surface (FS) sheet and two Q1D FS sheets, all mainly contributed by the Cr-3$d$ electrons. The penetration depth measurement [14] evidenced a nodal line in the pairing state below $T_c$. Meanwhile, the NMR experiment [15] revealed a power-law behavior of the spin-lattice relaxation rate, manifesting the 1D Luttinger liquid feature in the normal state. A couple of theoretical proposals have been devoted to the possible pairing symmetries of the superconducting state, concerning the respective relevance of the Q1D and 3D bands [16,17], while the formation of molecular orbital bands has been clarified in a twisted Hubbard tube [18]. These studies suggest possible competing superconducting and density-wave ordering tendencies in $K_2Cr_3As_3$. In fact, superconductivity associated with a magnetic quantum critical point has been revealed in the bulk materials of chromium arsenides [19,20]. Thus, the realization of density-wave instabilities competing with superconductivity in the Q1D chromium arsenide compounds is of interest and requires further studies.

Motivated by this issue, we studied the electronic and magnetic structures of a related compound, $KCr_3As_3$. This 133-type of chromium arsenide has recently been synthesized experimentally [21]. It consists of the Q1D $[CrAs]_\infty$ structure similar to $K_2Cr_3As_3$. The compound is metallic down to the lowest measured temperature, but no superconductivity has been observed. Instead, the polycrystal sample exhibits spin glass features at low temperatures [21]. Based on DFT calculations, we found that the electronic and magnetic structures of $KCr_3As_3$ exhibit new properties in contrast to the superconducting 233-type compound. The most prominent features are the disappearance of three-dimensional Fermi surface sheets and the emergence of the interlayer antiferromagnetic order. These numerical results indicate coexistence of local moments and itinerant electrons in the $KCr_3As_3$ compound due to the reduced dimensionality. Such exotic metallic magnetic phase could be attributed to the formation of high spin states in each Cr triangles via the orbital selective Mott transition. A frustration-induced quantum phase transition to the disordered low block-spin state with a spin gap is expected by tuning the intralayer exchange to the antiferromagnetic side. Our study thus reveals possible interplay between the unconventional superconductivity and the magnetic order in this class of materials.

## II. CALCULATION METHOD AND DETAILS

All reported results are obtained using the DFT as implemented in the Vienna *ab initio* simulation package (VASP) [22,23], where the valence electron-ion interactions are modeled using projected augmented wave (PAW) method [23,24] and the exchange-correlation effects are approximated with the Perdew-Burke-Enzerhoff (PBE) flavor of the general gradient approximation [25]. To ensure the convergence of the calculations, a 540 eV energy cutoff to the plane wave basis and a $6 \times 6 \times 12$ $\Gamma$-centered $K$ mesh is employed; whereas a $12 \times 12 \times 24$ $\Gamma$-centered $K$ mesh and tetrahedron method are employed to perform the DOS calculations.

*ccao@hznu.edu.cn

†daijh@hznu.edu.cn

 

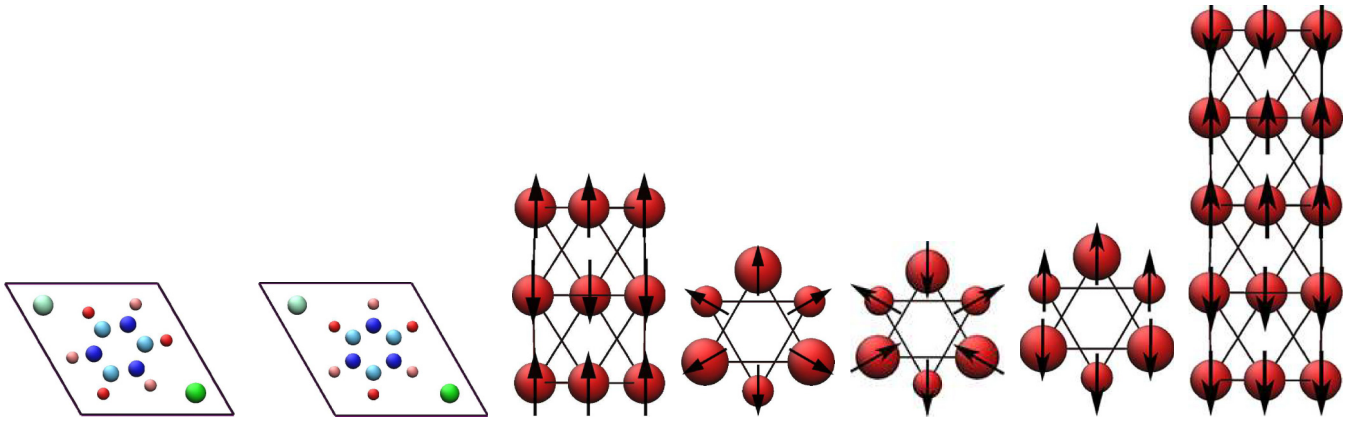


FIG. 1. (Color online) Crystal structure of $KCr_3As_3$ (a)–(b) and considered magnetic configurations (c)–(g). (a) Experimentally determined geometry with space group $P6_3/m$ (No. 176); (b) Hypothetic geometry closer to $K_2Cr_3As_3$ with space group P$\bar{6}$m2 (No. 187); (c) interlayer antiferromagnetic (IAF); (d) noncollinear antiferromagnetic (NCL); (e) in-out phase (IOP); (f) up-up-down phase (UUD); and (g) bilayer antiferromagnetic (BIAF). In (a) and (b), the red (smaller), blue (middle-sized), and green (larger) balls represents As, Cr, and K, respectively; darker and lighter colors indicate atoms at $z = 0.75$ ($X^{\mathrm{I}}$) and $z = 0.25$ ($X^{\mathrm{II}}$), respectively ($X$ = K, Cr, and As).

## III. RESULTS AND DISCUSSION

### A. Geometry and ground-state magnetism

Experimentally, the crystal structure of $KCr_3As_3$ shown in Fig. 1(a), was determined to be centrosymmetric with space group $P6_3/m$ (No. 176). Unlike the $K_2Cr_3As_3$ structure, the $Cr^{\mathrm{I}}$-$Cr^{\mathrm{I}}$ bond lengths are identical to the $Cr^{\mathrm{II}}$-$Cr^{\mathrm{II}}$ bond lengths in $KCr_3As_3$. Apart from this apparent difference, the $[CrAs]_6$ subnanotubes in $KCr_3As_3$ are rotated $\sim 10^\circ$ with respect to their central axis compared to the $K_2Cr_3As_3$ structure. In order to make connections with the 233-compound, we have also performed calculations on a hypothetical crystal structure of $KCr_3As_3$ which is initially with space group $P6_3/m$ (No. 176) but without the rotation of the $[CrAs]_6$ subnanotubes [Fig. 1(b)]. Interestingly, the symmetry of this structure spontaneously reduces to P$\bar{6}$m2 (No. 187) after optimization. So the loss of symmetric center is not due to the uneven distribution of K atoms between $z = 0.25$ and $z = 0.75$ planes in $K_2Cr_3As_3$, but is rather related to the rotation of the $[CrAs]_6$ subnanotubes.

Table I lists the total energies of $KCr_3As_3$ with different magnetic configurations within a single $[CrAs]_6$ tube. We shall show later that the intertube magnetic interactions are negligibly small, thus the intertube magnetic configurations are assumed to be ferromagnetic at this moment. In particular, we concentrated on the nonmagnetic (NM), ferromagnetic (FM), interlayer antiferromagnetic (IAF), in-out phase (IOP), and noncollinear antiferromagnetic (NCL) configurations [Figs. 1(c)–1(g)]. Unlike the $K_2Cr_3As_3$ compound, where multiple magnetic states are energetically almost degenerate in DFT calculations, the IAF configuration, a kind of block spin magnetic order, is apparently energetically much lower and is stable against structural optimization. Also, it is worth noting that both the noncollinear phases (IOP and NCL) are energetically much higher than the collinear phases (FM and IAF). Upon optimization, the collinear phases are stable while

TABLE I. Total energies of $KCr_3As_3$ with different magnetic configurations. The columns with (without) the superscription $^c$ are collinear (noncollinear) results obtained from calculations without (with) spin-orbit coupling, respectively. Rows Expt, Opt, and P$\bar{6}$m2 list the results with experimental lattice constants and coordinates, the optimized lattice constants and coordinates, and the hypothetical structure after optimization, respectively. Please note that the hypothetical structure was initially centrosymmetric $P6_3/m$ (No. 176), but spontaneously turned into P$\bar{6}$m2 (No. 187) after optimization. BIAF and UUD refer to bilayer antiferromagnetic configurations and up-up-down configurations, respectively (Ref. [46]).

| | | FM | IAF | IOP | NCL | NM | BIAF$^c$ | UUD$^c$ | FM$^c$ | IAF$^c$ | NM$^c$ |
|---|---|---|---|---|---|---|---|---|---|---|---|
| | $a$ ($c$) | 9.0886 (4.1801) | | | | | 9.0886 (4.1801) | | | | |
| Exp | $\Delta E$ (meV) | −41.3(−43.9) | −121.7(−119.4) | −22.5 | −16.0 | 0.0 | −20.7 | −23.4 | −50.7 | −129.7 | 0.0 |
| | $m_{\mathrm{Cr}}$ ($\mu_B$) | 0.36 | 0.77 | 0.51 | 0.31 | 0.00 | 0.44 | 0.40 | 0.37 | 0.78 | 0.00 |
| | $a$ ($c$) | 9.3442 (4.0862) | 9.3419 (4.0974) | to NM | | 9.3447 (4.0826) | | | | | |
| Opt | $\Delta E$ (meV) | −0.8(−6.0) | −20.4 | to NM | | 0.0 | | | | | |
| | $m_{\mathrm{Cr}}$ ($\mu_B$) | 0.14 | 0.29 | to NM | | 0.0 | | | | | |
| | $a$ ($c$) | 9.7091 (4.0848) | 9.7067 (4.0904) | to NM | | 9.7109 (4.0826) | | | | | |
| P$\bar{6}$m2 | $\Delta E$ (meV/Cr) | −1.6(−4.1) | −7.0 | to NM | | 0.0 | | | | | |
| | $m_{\mathrm{Cr}}$ ($\mu_B$) | 0.1 | 0.24(-0.29) | to NM | | 0.00 | | | | | |

the noncollinear ones are not. For the lowest-energy state IAF, the magnetic moment on each Cr is calculated to be ∼0.77 $\mu_B$, in agreement with the experimental observation of 0.68 $\mu_B$ [21].

### B. Electronic Structure

In order to understand the formation of magnetic moments, we first examine the electronic structure of $KCr_3As_3$ in the nonmagnetic state. As shown in Fig. 2(a), the band structure of $KCr_3As_3$ near the Fermi level is quite similar to that of $K_2Cr_3As_3$, including the orbital characters. However, the degeneracies at Γ and K are completely different. Indeed, the degeneracies at K and the twofold degeneracy of the $KCr_3As_3$ bands around $E_F$-0.5 eV at $k_z = 0.5$ (A-H-L-A) are direct consequences of the $S_6$ symmetry, which is broken in $K_2Cr_3As_3$. Furthermore, the reduction of 50% potassium atoms causes hole doping to the system, resulting in a shift of the Fermi level. As a result, the number of bands cross the Fermi level becomes five, among which three are quasi-1D and two are 3D. The DOS and the orbital contributions are shown in Fig. 2(b). The quasi-1D signature van Hove singularities are apparent around −1.6 eV, −0.5 eV, −0.4 eV, 0.5 eV relative to $E_F$. The DOS around $E_F$ is dominated by the Cr-3$d$ orbitals, in particular, Cr-3$d_{xy}$ and 3$d_{x^2-y^2}$ orbitals. By integrating the PDOS of Cr-3$d_{xy}$ and 3$d_{x^2-y^2}$ orbitals to the Fermi level, ∼0.8 electron per orbital can be obtained. The contribution of Cr-3$d_{z^2}$ orbital is small, but non-negligible since the $\alpha$ band is almost exclusively contributed by Cr-3$d_{z^2}$ [Fig. 2(a)]. The Fermi surface (FS) of $KCr_3As_3$ constitutes of three quasi-1D sheets and two 3D sheets [Fig. 2(c)]. If the system is doped with one electron per formula (i.e., $K_2Cr_3As_3$), the FS sheets will be reduced to two quasi-1D and one 3D, as in the original $K_2Cr_3As_3$ compound [9]. Of course, the shape of the 3D FS sheet is different from that in the original $K_2Cr_3As_3$ due to the local structure difference.

We now show the electronic structure of the lowest interlayer antiferromagnetic phase (IAF) in Figs. 3(a)–3(b). The orbital characteristics of bands near $E_F$ remains the same as those in the NM state. The four Cr-3$d_{x^2-y^2}$/Cr-3$d_{xy}$ bands near $E_F$ are separated by ∼0.4 eV in the IAF phase, presumably due to the formation of magnetic moment on Cr; whereas these bands are very close to each other in the NM phase. As a result, two of these bands, who formed the 3D FS sheets in the NM phase, become fully occupied, leaving us only three quasi-1D sheets in the IAF phase [Fig. 3(c)]. It is worth noting that the band around $E_F$-0.03 eV are very flat, yielding strong quasi-1D van Hove singularity in the DOS [Fig. 3(b)]. We should also emphasize that these two occupied Cr-3$d_{x^2-y^2}$/Cr-3$d_{xy}$ bands are strongly spin-polarized and appears to be localized around the Cr atoms, thus contribute to the possible local moments of the system [Fig. 3(d)].

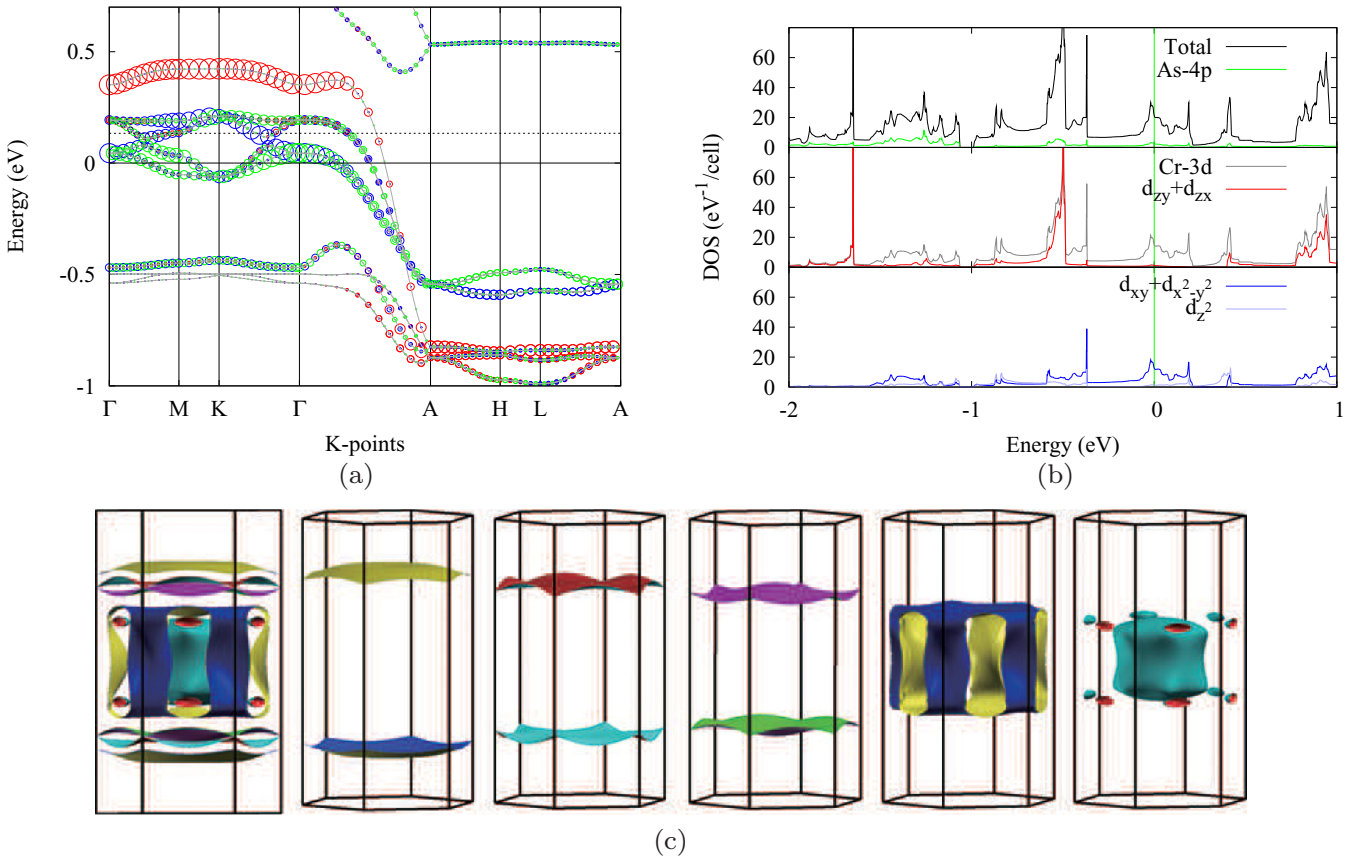


FIG. 2. (Color online) (a) Band structure, (b) density of states, and (c) Fermi surfaces of nonmagnetic $KCr_3As_3$. In (a), the size of the red/blue/green circles are proportional to the orbital weight of the Cr-3$d_{z^2}$/-3$d_{x^2-y^2}$/-3$d_{xy}$, respectively. The dashed horizontal line indicates the Fermi level corresponding to doping the system with one electron/formula, i.e., $K_2Cr_3As_3$.

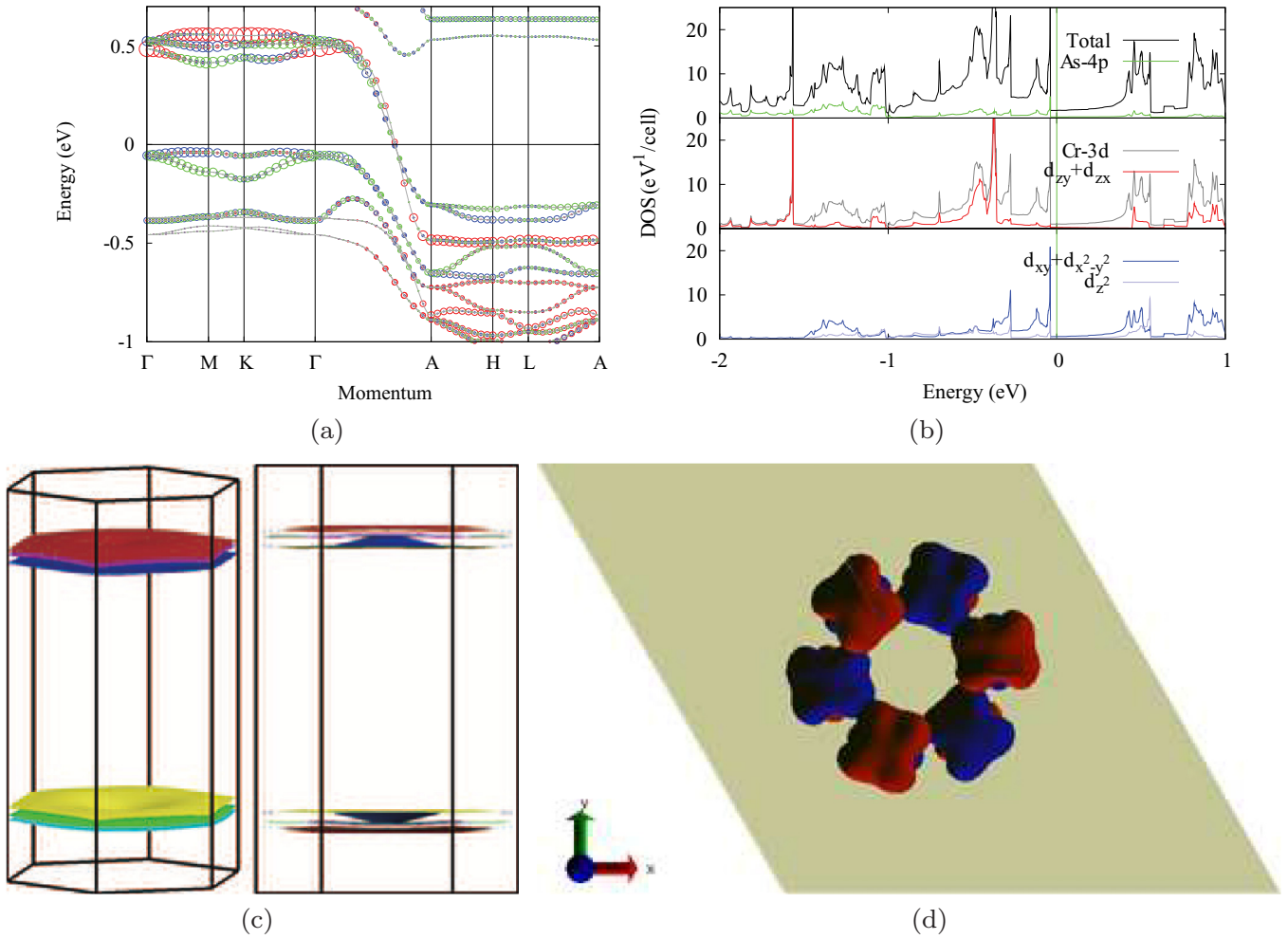


FIG. 3. (Color online) (a) Band structure, (b) density of states, and (c) Fermi surfaces of $KCr_3As_3$ in the IAF state. (d) Real-space charge density of the two filled Cr-$3d_{x^2-y^2}$/-$3d_{xy}$ bands from $E_F$-0.7 eV to $E_F$-0.03 eV. In (a)–(c), only spin up channel is shown for clarity purposes. In (a), the size of the red/blue/green circles are proportional to the orbital weight of the Cr-$3d_{z^2}$/-$3d_{x^2-y^2}$/-$3d_{xy}$, respectively. In (d) Red and blue contour denote spin-up and spin-down electron, respectively; and the contour is taken at $\rho = 0.1\rho_{\max}$.

### C. Magnetic frustration

The above DFT calculations suggest the possibility of local moments in $Cr_3As_3$, given the facts that the calculated magnetic moment $\sim 0.77\mu_B$ is close to the saturated value of $S = 1/2$ isolated local moment and quantum frustrations are not considered so far. One possible route to understand the formation of the possible local moments in such system may involve the orbital selective Mott transition [26,27] as in iron pnictides [28–30]. By examining the nonmagnetic band structure Fig. 2(a), one could notice two upper degenerate bands along the $\Gamma \to A$ direction intersect the Fermi energy at the Fermi point $k_{F_z} \sim 0.56\pi$, close to $\pi/2$ and indicating the nearly half-filling case of the corresponding molecular orbital band. In pure one dimension, any repulsive Coulomb interaction will induce $4k_{F_z}$ umklapp scattering at half filling, resulting in a finite charge gap. Therefore, a Mott transition in this band is naturally expected before the formation of the corresponding molecular orbital bands [18]. Of course, there may be other possible phases in Q1D systems, such as density-wave orders or anisotropic metals. But compared with the band structure of $K_2Cr_3As_3$, both the band narrowing effect and the electron correlations are enhanced due to the reduced dimensionality in $KCr_3As_3$, rendering the Q1D Mott phase more possible.

We then consider a local moment at each Cr site described by a spin operator, $\mathbf{S_r}$, with the magnitude $S = 1/2$. Assuming that the coupling between itinerant electrons and local moments is relatively weak, we consider the Hamiltonian of the localized spins within one $[CrAs]^{\infty}$ tube as

$$\mathcal{H}_{\text{spin}} = J_1 \sum_{n,i,j} \mathbf{S}_{n,i} \cdot \mathbf{S}_{n,j} + \tilde{J}_1 \sum_{n,i',j'} \mathbf{S}_{n,i'} \cdot \mathbf{S}_{n,j'} + J_2 \sum_{n,i,j'} \mathbf{S}_{n,i} \cdot \mathbf{S}_{n,j'} + \tilde{J}_2 \sum_{n,i,j'} \mathbf{S}_{n,i} \cdot \mathbf{S}_{n+1,j'}, \quad (1)$$

where $n$ is the unit-cell index; $i$, $j$ and $i'$, $j'$ denote the Cr sites in the two conjugated triangles, respectively. Thus, the first two terms indicate the intralayer nearest-neighbor couplings in the two different triangles, while the last two terms the interlayer nearest-neighbor couplings between the two triangles within one unit cell and across two unit cells, respectively.

The spin model is an extended variant of twisted spin tubes previously proposed for the three-leg systems $[(CuCl_2tachH)_3]Cl_2$ and $CsCrF_4$ [31–34]. The magnetic frustrations will arise not only due to the intralayer spin exchanges but also the interlayer or inter-unit-cell spin exchanges if they are all antiferromagnetic. Concerning the present $KCr_3As_3$ compound, we can assume $J_1 = \tilde{J}_1$, $J_2 = \tilde{J}_2$. Their values are estimated by fitting the corresponding energies in different magnetic structures with the moment per Cr atom being fixed at 0.77 $\mu_B$. The variations of the Cr-3$d$ orbital occupations are found to be less than 0.1 e per atom in these calculations. The best fitting suggests $J_1 = -9.9\,\mathrm{meV}/S^2$ and $J_2 = 18.5\,\mathrm{meV}/S^2$.[1] It is worth noting here that we have also determined the strength of the intertube interaction $J_t$ for the IAF state to be $J_t \sim 1$ meV by comparing the DFT total energies of intertube-FM and intertube-AFM states. Hence $J_t$ is much weaker and is neglected for the moment. The ferromagnetic $J_1$ implies the suppression of the magnetic frustration in this 133-compound. In this case, the twisted tube is basically a rhombus lattice without frustration due to the bipartite nature of the lattice. A large block-spin $S_\triangle = 3/2$ state is then expected for each Cr triangle, involving the four polarization components: $|\frac{3}{2}\rangle = |\uparrow\uparrow\uparrow\rangle$, $|-\frac{3}{2}\rangle = |\downarrow\downarrow\downarrow\rangle$, $|\frac{1}{2}\rangle = \frac{1}{\sqrt{3}}[|\uparrow\uparrow\downarrow\rangle + |\uparrow\downarrow\uparrow\rangle + |\downarrow\uparrow\uparrow\rangle]$, $|-\frac{1}{2}\rangle = \frac{1}{\sqrt{3}}[|\uparrow\downarrow\downarrow\rangle + |\downarrow\uparrow\downarrow\rangle + |\downarrow\downarrow\uparrow\rangle]$. By introducing a spin-3/2 operator $\mathcal{T}$ acting on these $S_\triangle = 3/2$ states, we obtain the effective Hamiltonian

$$\mathcal{H}_{S_\triangle=3/2} = \sum_n [K_1 \mathcal{T}_n \cdot \mathcal{T}_{n+1} + K_2 (\mathcal{T}_n \cdot \mathcal{T}_{n+1})^2] \qquad (2)$$

with $K_1 = 2J_2/3 + J_2^2/(18|J_1|)$ and $K_2 = -J_2^2/(54|J_1|)$ [35]. The low-temperature property is dominated by the $K_1$ term. For the pure 1D spin tube, $J_t = 0$, the interlayer antiferromagnetic order is only quasi-long-ranged, in the sense that the spin-spin correlation function exhibits a power-law behavior and the spin excitation spectrum is gapless. But for the Q1D spin tube, a very small $|J_t|$ will lead to the interlayer ordering at a finite though reduced transition temperature.

This magnetic ground state remains stable in a wider parameter regime when $J_1$ moves toward the antiferromagnetic side. However, when $J_1$ is much larger than $J_2$, the ground state will be changed due to strong frustrations. In the limiting case, each triangle can be solved independently, giving rise to the doubly degenerated ground states involving $|\uparrow_R\rangle = \frac{1}{\sqrt{3}}[|\uparrow\uparrow\downarrow\rangle + \omega|\uparrow\downarrow\uparrow\rangle + \omega^{-1}|\downarrow\uparrow\uparrow\rangle]$, $|\uparrow_L\rangle = \frac{1}{\sqrt{3}}[|\uparrow\uparrow\downarrow\rangle + \omega^{-1}|\uparrow\downarrow\uparrow\rangle + \omega|\downarrow\uparrow\uparrow\rangle]$ (and the states with $|\uparrow\rangle \Leftrightarrow |\downarrow\rangle$). Noted that these lower block-spin $S_\triangle = 1/2$ states are chiral in nature, associated with the $C_3$ rotation $\omega = e^{i2\pi/3}$. To the lowest order in $J_2$, the effective spin model describing these $S_\triangle = 1/2$ spin excitations is given by [36,37]

$$\mathcal{H}_{S_\triangle=1/2} = \frac{2J_2}{3} \sum_n \mathbf{T}_n \cdot \mathbf{T}_{n+1} [1 + 2(\omega^2 \tau_n^+ \tau_{n+1}^- + \mathrm{H.c.})],$$

with $\mathbf{T}$ being a spin-1/2 operator acting on the two different spin polarization components $\sigma = \uparrow, \downarrow$, while $\tau^\pm$ on the chirality degrees of freedom, namely, $\tau^+|\sigma L\rangle = 0, \tau^-|\sigma R\rangle = |L\rangle, \tau^+|\sigma R\rangle = |L\rangle, \tau^-|\sigma R\rangle = 0$. According to earlier numerical studies, this model has a disordered ground state, i.e., the dimerized ground state exhibiting gaps in both spin and chirality excitations [36,37].

It is well known from the celebrated Lieb-Schultz-Mattis theorem [38] that half-spin chains have either a degenerated ground state or gapless spin spectrum. Interestingly, with increasing ratio $\alpha = J_2/J_1$, both situations could be realized in the present material. The quantum phase transition from gapless to gapful phases takes place around $\alpha_c \sim 1.22$ [35,39].

## IV. SUMMARY AND CONCLUSION

Our DFT calculations show that the ground state of the $KCr_3As_3$ compound is metallic and extremely Q1D compared with its superconducting $K_2Cr_3As_3$ counterpart. Moreover, it exhibits an interlayer antiferromagnetic order with a large block-spin $3 \times 0.77\mu_B \sim 2.3\mu_B$ in each Cr triangles. By fitting the twisted $J_1$-$J_2$ spin tube model, we find that the basic magnetic property can be actually captured by the antiferromagnetic Heisenberg chain with block-spin $S_\triangle = 3/2$ defined in Eq. (2). The calculated magnetic moment and dominating antiferromagnetic intratube interaction $J_2$ are in reasonable agreement with the susceptibility measurement where the effective moment is about 0.68 $\mu_B$/Cr and the Curier-Weiss temperature is $-83$ K [21]. The intertube interaction, although it is much smaller than the intratube interactions, could stabilize the long-range magnetic order at low temperatures. The absence of superconductivity is likely due to the strong competition tendency of 133-compound to have an antiferromagnetic order.

We should remark that the spin glass behavior, instead of the static magnetic order, was observed in the polycrystalline samples [21]. This is most likely due to the disorder effect, which can in turn render the antiferromagnetic order short ranged and induce a spin glass behavior [40,41]. We also remark here that although the ground state is gapless, the lower spin $S_\triangle = 1/2$ sector may still play some role at finite temperatures, exhibiting a crossover-to-spin-gap behavior as in the spin tube material $[(CuCl_2tachH)_3]Cl_2$ [42].

An intriguing situation could be expected with a large intralayer antiferromanetic coupling $J_1$ while keeping the symmetry of charge distributions between the two conjugated triangles. Such situation should be contrasted to the 233-compound, where the more $K$ concentration induces the noncentrosymmetric structural distortion and asymmetric charge distributions in the two conjugated triangles. Because superconductivity may be also induced from the spin-gapped phase upon doping [43] and given the recent pressure experiments on the $K_2Cr_3As_3$ [44,45], we expect that the disordered phase with both spin and chirality gaps can be realized in further coming pressure experiments on $KCr_3As_3$ and the related compounds.

## ACKNOWLEDGMENTS

The authors would like to thank Guanghan Cao, Jiangping Hu, Zhong-Yi Lu, Qimiao Si, Zhuan Xu, Fuchun

[1] The exchange coupling constants $J_1$ and $J_2$ were fitted using the least-square fitting method. The best fitting yields a coefficient of determination of 89.77%, and the error introduced by pseudopotential method is estimated to be $\sim$ 2meV.

Zhang, and Yi Zhou for inspiring discussions. This work has been supported by the NSFC (Grants No. 11274006, No. 11274084, and No. 11304071), National Basic Research Program (Grant No. 2014CB648400) and the Zhejiang Provincial Natural Science Foundation (Grant No. LR12A04003). All calculations were performed at the High Performance Computing Center of Hangzhou Normal University College of Science.

[1] P. C. Hohenberg, Phys. Rev. **158**, 383 (1967).
[2] N. D. Mermin and H. Wagner, Phys. Rev. Lett. **17**, 1133 (1966).
[3] D. Jérome, A. Mazaud, M. Ribault, and K. Bechgaard, J. Phys. Lett. France **41**, 95 (1980).
[4] R. Brusetti, P. Monceau, M. Potel, P. Gougeon, and M. Sergent, Solid State Commun. **66**, 181 (1988).
[5] M. Greenblatt, W. McCarroll, R. Neifeld, M. Croft, and J. Waszczak, Solid State Commun. **51**, 671 (1984).
[6] J.-F. Mercure, A. F. Bangura, X. Xu, N. Wakeham, A. Carrington, P. Walmsley, M. Greenblatt, and N. E. Hussey, Phys. Rev. Lett. **108**, 187003 (2012).
[7] H. Wilhelm, D. Jaccard, R. Duprat, C. Bourbonnais, D. Jérome, J. Moser, C. Carcel, and J. Fabre, Eur. Phys. J. B **21**, 175 (2001).
[8] C. Bourbonnais and D. Jerome, *Physics of Organic Superconductors and Conductors* (Springer, Berlin, 2008), Vol. 110, pp. 357–412.
[9] J.-K. Bao, J.-Y. Liu, C.-W. Ma, Z.-H. Meng, Z.-T. Tang, Y.-L. Sun, H.-F. Zhai, H. Jiang, H. Bai, C.-M. Feng *et al.*, Phys. Rev. X **5**, 011013 (2015).
[10] Z.-T. Tang, J.-K. Bao, Y. Liu, Y.-L. Sun, A. Ablimit, H.-F. Zhai, H. Jiang, C.-M. Feng, Z.-A. Xu, and G.-H. Cao, Phys. Rev. B **91**, 020506 (2015),
[11] Z.-T. Tang, J.-K. Bao, Z. Wang, H. Bai, H. Jiang, Y. Liu, H.-F. Zhai, C.-M. Feng, Z.-A. Xu, and G.-H. Cao, Sci. China Mater. **58**, 16 (2015).
[12] H. Jiang, G.-H. Cao, and C. Cao, Sci. Rep. **5**, 16054 (2015).
[13] X.-X. Wu, C.-C. Le, J. Yuan, H. Fan, and J.-P. Hu, Chin. Phys. Lett. **32**, 057401 (2015).
[14] G. M. Pang, M. Smidman, W. B. Jiang, J. K. Bao, Z. F. Weng, Y. F. Wang, L. Jiao, J. L. Zhang, G. H. Cao, and H. Q. Yuan, Phys. Rev. B **91**, 220502(R) (2015).
[15] H.-Z. Zhi, T. Imai, F.-L. Ning, J.-K. Bao, and G.-H. Cao, Phys. Rev. Lett. **114**, 147004 (2015).
[16] Y. Zhou, C. Cao, and F.-C. Zhang, arXiv:1502.03928.
[17] X. Wu, F. Yang, C. Le, H. Fan, and J. Hu, Phys. Rev. B **92**, 104511 (2015).
[18] H. Zhong, X.-Y. Feng, H. Chen and J. Dai, Phys. Rev. Lett. **115**, 227001 (2015).
[19] W. Wei *et al.*, Nature Commun. **5**, 5508 (2014).
[20] H. Kotegawa, N. Nakahara, H. Tou, and H. Sugawara, J. Phys. Soc. Jpn. **83**, 093702 (2014).
[21] J.-K. Bao, L. Li, Z.-T. Tang, Y. Liu, Y.-K. Li, H. Bai, C.-M. Feng, Z.-A. Xu, and G.-H. Cao, Phys. Rev. B **91**, 180404 (2015).
[22] G. Kresse and J. Hafner, Phys. Rev. B **47**, 558 (1993).
[23] G. Kresse and D. Joubert, Phys. Rev. B **59**, 1758 (1999).
[24] P. E. Blöchl, Phys. Rev. B **50**, 17953 (1994).
[25] J. P. Perdew, K. Burke, and M. Ernzerhof, Phys. Rev. Lett. **77**, 3865 (1996).
[26] A. Liebsch, Phys. Rev. B **70**, 165103 (2004).
[27] L. de Medici, S. R. Hassan, M. Capone, and X. Dai, Phys. Rev. Lett. **102**, 126401 (2009).
[28] R. Yu and Q. Si, Phys. Rev. B **86**, 085104 (2012).
[29] B. Valenzuela, M. J. Calderon, G. Leon, and E. Bascones, Phys. Rev. B **87**, 075136 (2013).
[30] J. Rincon, A. Moreo, G. Alvarez, and E. Dagotto, Phys. Rev. Lett. **112**, 106405 (2014).
[31] G. Seeber, P. Kogerler, B. M. Kariuki, and L. Cronin, Chem. Commun. **14**, 1580 (2004).
[32] J. Schnack, H. Nojiri, P. Kögerler, G. J. T. Cooper, and L. Cronin, Phys. Rev. B **70**, 174420 (2004).
[33] H. Manaka, Y. Hirai, Y. Hachigo, M. Mitsunaga, M. Ito, and N. Terada, J. Phys. Soc. Jpn. **78**, 093701 (2009).
[34] T. Sakai, M. Sato, K. Okamoto, K. Okunishi, and C. Itoi, J. Phys.: Condens. Matter **22**, 403201 (2010).
[35] J.-B. Fouet, A. Läuchli, S. Pilgram, R. M. Noack, and F. Mila, Phys. Rev. B **73**, 014409 (2006).
[36] K. Kawano and M. Takahashi, J. Phys. Soc. Jpn. **66**, 4001 (1997).
[37] A. Lüscher, R. M. Noack, G. Misguich, V. N. Kotov, and F. Mila, Phys. Rev. B **70**, 060405 (2004).
[38] E. Lieb, T. Schultz, and D. Mattis, Ann. Phys. (N.Y.) **16**, 407 (1961).
[39] K. Okunishi, S. Yoshikawa, T. Sakai, and S. Miyashita, Prog. Theor. Phys. Suppl. **159**, 297 (2005).
[40] K. Binder and A. P. Young, Rev. Mod. Phys. **58**, 801 (1986).
[41] J. A. Mydosh, Rep. Prog. Phys. **78**, 052501 (2015).
[42] N. B. Ivanov, J. Schnack, R. Schnalle, J. Richter, P. Kögerler, G. N. Newton, L. Cronin, Y. Oshima, and H. Nojiri, Phys. Rev. Lett. **105**, 037206 (2010).
[43] T. M. Rice, S. Gopalan, and M. Sigrist, Europhys. Lett. **23**, 445 (1993).
[44] T. Kong, S. L. Bud'ko, and P. C. Canfield, Phys. Rev. B **91**, 020507(R) (2015).
[45] Z. Wang, V. Sidorov, Q. Wu, J. Bao, Z. Tang, W. Yi, J. Guo, Y. Zhou, S. Zhang, C. Zhang *et al.*, arXiv:1502.04304.